Special Issue: Sars-CoV-2 Epidemic

Vol. 4, No. 1 (2020)
ISSN: 2532-5876
Open access journal licensed under CC-BY
DOI: 10.13133/2532-5876/16968

COVID-19 Calls for Mathematics, Part 1: Neuraminidase Inhibitors, Chloroquine and Hydroxychloroquine

Corrado Mascia[a], Veronica Paparozzi[a], Angelica Ragni[a], Elisa Scanu[a], Chiara Simeoni[b] and Elisa Tomellini[a]*

[a] *Dipartimento di Matematica G. Castelnuovo, Sapienza Università di Roma, Italy*
[b] *Laboratoire de Mathématiques J.A. Dieudonné CNRS UMR 7351, Université Côte d'Azur, Parc Valrose - 06108 Nice Cedex 2, France*

Corresponding authors: Corrado Mascia, corrado.mascia@uniroma1.it, Chiara Simeoni, chiara.simeoni@univ-cotedazur.fr

Abstract
Looking at the outbreak of SARS-CoV-2 and the global state of emergency imposed due to its pandemic spread, the necessity for antiviral drugs to be immediately available is a priority for the scientific community. Considering that research and implementation of new antiviral therapies or vaccines usually take a long time, the World Health Organization (WHO) has proposed to use in commerce drugs: in fact, repurposing drugs which are already accessible in large quantities is easier to fight against the virus, at least during the first emergency phase. In this article, we discuss various mathematical models which simulate the action of antiviral drug therapies, such as neuraminidase inhibitors (NIs), for the treatment of H1N1 Influenza A virus, by using data collected through in vitro and in vivo experiments. This constitutes a paradigmatic case of study for paving the way to a systematic investigation of the effects of chloroquine and hydroxychloroquine as therapeutics in the treatment of SARS-CoV-2.

Keywords: SARS-CoV-2, Influenza A virus, basic reproduction number, neuraminidase inhibitors, interferon-mediated immune response, target cell-limited model, antiviral treatments, chloroquine and hydroxychloroquine, numerical simulations, experimental data

Citation: Mascia, C, Paparozzi, V, Ragni, A, Scanu, E, Simeoni, C, Tomellini, E, 2020, "COVID-19 Calls for Mathematics, Part 1: Neuraminidase Inhibitors, Chloroquine and Hydroxychloroquine", *Organisms: Journal of Biological Sciences*, vol. 4, no. 1, pp. 115-127. DOI: 10.13133/2532-5876/16968.

1. Mathematical modeling of influenza: a virus dynamics

Given the current lack of a vaccine for Severe Acute Respiratory Syndrome Coronavirus 2 (SARS-CoV-2), the virus causing COVID-19, it is worthwhile evaluating potential prophylactic or therapeutic effects of drugs which are clinically approved for other indications. Chloroquine, and its derivative hydroxychloroquine (HCQ), have been already used with good results for the treatment of malaria and also in some autoimmune diseases, with the most common side effect being eye damage after heavy dosage and long-term administration [5]. The precise mechanisms through which chloroquine may act to attenuate SARS-CoV-2 infection are of considerable interest, as this information could be valuable for identifying new treatments, while waiting for a vaccine.

Chloroquine is a weak base which becomes entrapped in membrane-enclosed low pH organelles, interfering with their acidification [17]. Chloroquine accumulates in the digestive vacuole of infected cells, in which the treatment leads to an increase of lysosomal pH. Speculation on chloroquine-induced antiviral effects hence include inhibition of pH-dependent viral fusion/replication and prevention of receptor binding by viral envelope glycoproteins; chloroquine may also inhibit virions assembly in endoplasmic reticulum Golgi intermediate compartment (ERGIC). Moreover, due to its potentiality in diminishing the expression of pro-inflammatory factors and receptors, such as cytokines, chloroquine has already been proposed in 2003 as treatment for SARS [17], which is primarily responsible for coronavirus-associated mortality.

It has been demonstrated that chloroquine is a broad-spectrum inhibitor of nanoparticle endocytosis by resident macrophages, since chloroquine decreases the accumulation of some synthetic nanoparticles in cell lines [23, 16]. Indeed, mechanistic studies have revealed that chloroquine reduces the expression of phosphatidylinositol binding clathrin assembly protein (PICALM), which is a cargo-selecting clathrin adaptor sensing and driving membrane curvature, thereby regulating the rate of endocytosis [14]. If PICALM runs out, then the clathrin-mediated endocytosis, which is a predominant pathway for synthetic nanoparticle internalization, is inhibited. Furthermore, chloroquine is known to prevent lysosome acidification, which is likely to interfere with upstream endocytic trafficking, causing a 'traffic jam' scenario that blocks effective transport of cargo to and from the cell membrane [23, 16].

It has been shown that SARS-CoV-2 falls within the same size range (60-140 nm) and shape (spherical) as commonly studied synthetic nanoparticles [24], which are typically sensible to chloroquine action [16, 9]. Therefore, one of the mechanisms responsible for chloroquine-mediated effects against SARS-CoV-2 could be a general decrease in the ability of cells to perform endocytosis. Moreover, previous studies for SARS-CoV-1 infection [10, 22] are possibly useful also for SARS-CoV-2, since these two viruses might employ similar angiotensin-converting enzyme 2 (ACE2) mediated mechanisms of cell entry. Even if chloroquine mechanism of lysosome acidification is likely to interfere with

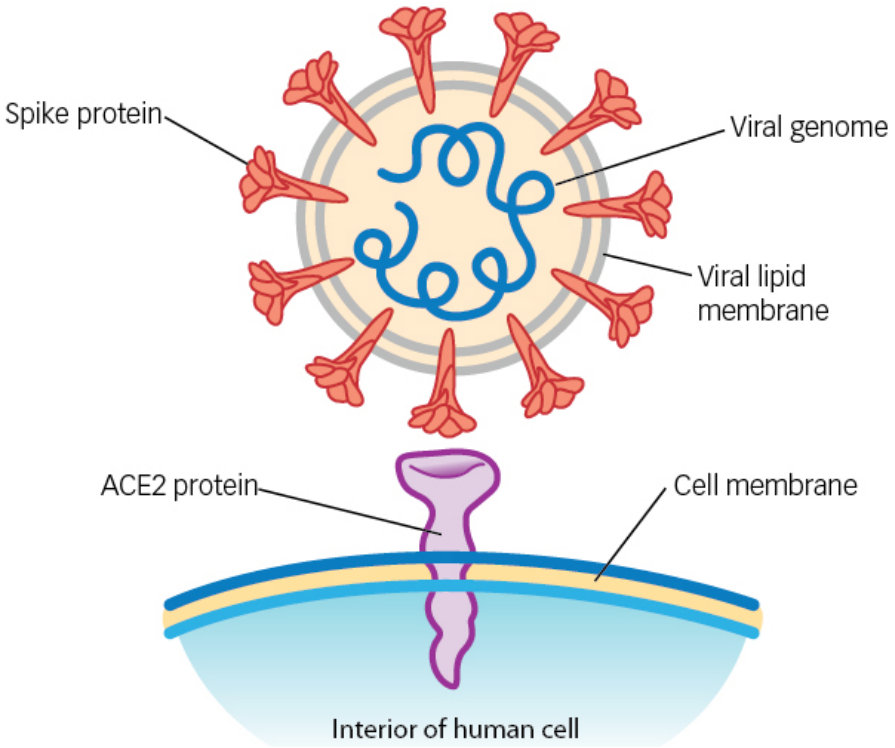

Figure 1: SARS-CoV-2 enters human cells using spike proteins as a bridge between viral envelope and cell membrane – www.perioimplantadvisory.com/periodontics/oral-medicine-anesthetics-and-oral-systemic-connection/article/14173521/covid19-and-the-problem-with-dental-aerosols.

the action of membrane receptors, previous studies have revealed that chloroquine has therapeutic activity against SARS-CoV in cell culture but does not alter cell-surface levels of ACE2 [20]. Additionally, it has been proven that therapeutic doses of chloroquine do not substantially change the biosynthesis or glycosylation of the SARS-CoV spike glycoprotein [20], which is fundamental for virus entry into cells. On the contrary, this antiviral might have an important role in preventing the entry of virions in cells. Indeed, lysosomal acidification is responsible of a conformational change in the spike protein, bridging the viral envelope and the endosomal membrane together to enable fusion; thus, chloroquine-induced inhibition of endosomal acidification is likely to alter this fusion event, stalling the virus in endosomes (see Figure 1).

However, the use of chloroquine has some serious limitations, because part of its pharmacokinetics remains unknown, and its real efficacy is still not well defined [9, 19, 4].

As paradigmatic case of study, we discuss a mathematical model which illustrates the action of neuraminidase inhibitors (NIs), such as Zanamivir, for the treatment of H1N1 Influenza A virus, according to the results by Baccam et al. [1]. This model has been introduced to analyze the virus kinetics in the upper respiratory tracts of infected adults, by focusing on the importance of immune response to better fit with available experimental data. When we do not consider the application of antiviral treatments, the so-called *target cell-limited model with eclipse phase* is given by the following ordinary differential equations:

$$\begin{cases} \dfrac{dT}{dt} = -\beta T V \\ \dfrac{dI_1}{dt} = \beta T V - k I_1 \\ \dfrac{dI_2}{dt} = k I_1 - \delta I_2 \\ \dfrac{dV}{dt} = p I_2 - c V \end{cases} \tag{1}$$

where T is the number of uninfected target cells, I_1 is the number of infected cells not yet producing virus (i.e. in the eclipse phase), I_2 is the number of infected cells actively producing virus, and V denotes the infectious-viral titer expressed in TCID50/ml of nasal

patient	V_0 TCID50/ml	β $d^{-1}(\text{TCID50/ml})^{-1}$	k d^{-1}
1	4.3×10^{-2}	4.9×10^{-5}	3.9
2	3.1×10^{-7}	1.1×10^{-3}	2.0
3	7.0×10^{-1}	1.7×10^{-4}	4.9
4	4.9	5.3×10^{-6}	4.0
5	1.7	2.7×10^{-6}	6.0
6	2.4	8.4×10^{-6}	4.4

patient	p d^{-1}	c d^{-1}TCID50/ml	δ d^{-1}	R_0
1	4.2	2.8×10^{-2}	4.3	30.4
2	10.9	2.1×10^{-2}	11.0	77.1
3	2.3	3.0×10^{-3}	2.2	40.3
4	3.8	1.3×10^{-1}	3.8	19.1
5	13.5	5.9×10^{-1}	13.5	3.5
6	3.8	7.1×10^{-2}	3.7	17.0

Table 1: Patient-specific best-fit parameter values for the target cell-limited model (1) as found in [1].

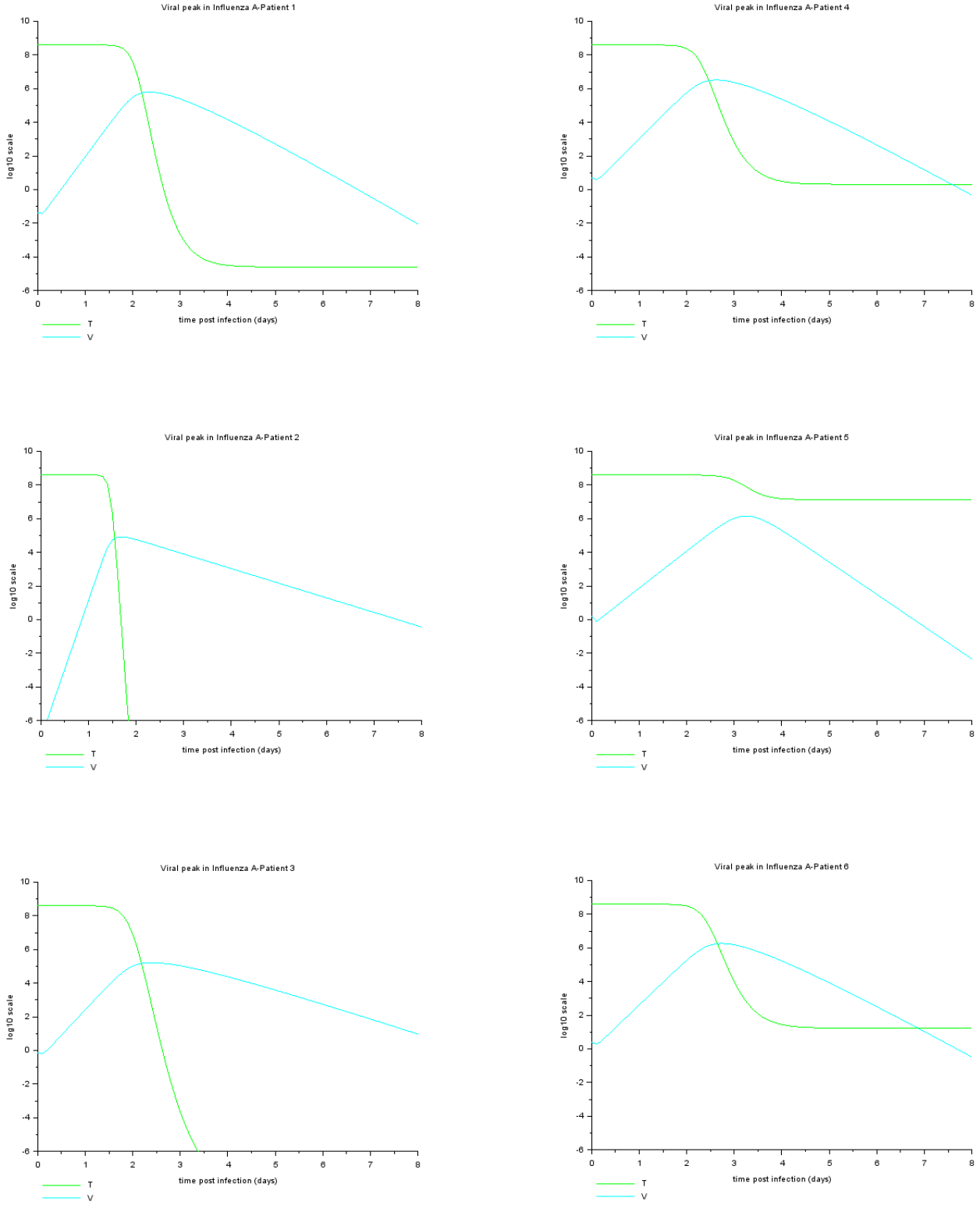

Figure 2: Viral titer in TCID50/ml of nasal wash and fraction of target cells remaining over the course of infection (8 days) in six different patients, corresponding to the experimental data in Table 1.

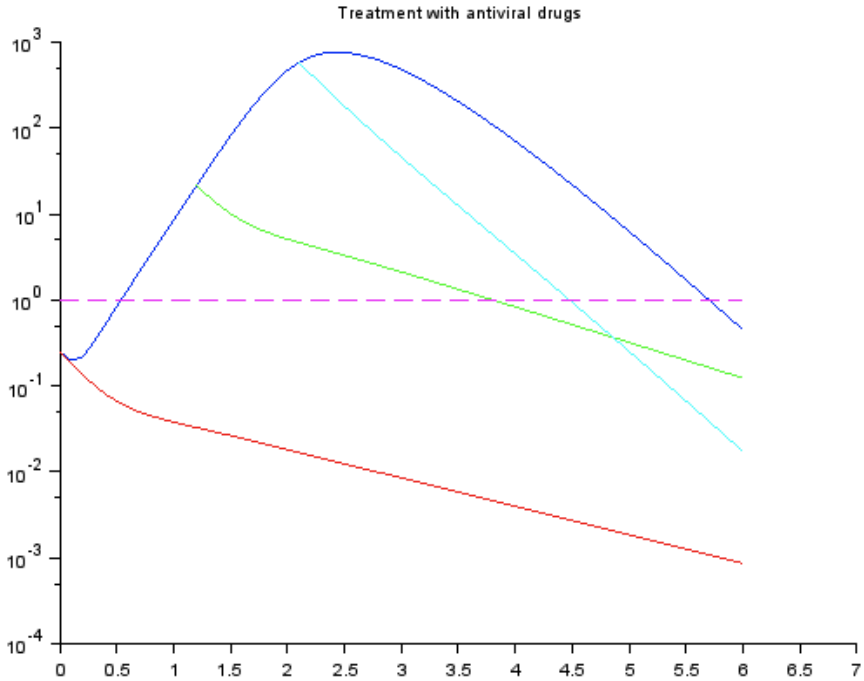

Figure 3: Course of Influenza A virus infection with and without the neuraminidase inhibitor Zanamivir administrated intranasally. The predicted virus titer dynamics from model (1) is shown for the placebo group (blue), the delayed-treatment group (light blue), the early-treatment group (green) and the preventive-treatment group (red). The horizontal magenta line marks the experimental limit of detection for the viral titer. We take the initial data for the green curve at time 1:2 of the placebo group and for the light blue curve at time 2.08 of the placebo group, together with 0.03 x p as virus production rate (that is because we suppose an instantaneous change of p value due to the antiviral administration with respect to previous placebo patients, and the system (1) is actually time-autonomous).

wash. The parameter β represents the constant rate characterizing the infection of target cells, which become infected cells in the eclipse phase (I_1), successively transforming into cells which actively produce virus (I_2) with an average transition time $1/k$. In turn, these cells increase the viral titer (V) by releasing virions at an average rate p (per cell), and die at a rate δ (per cell), thus $1/\delta$ is the average life span of a productively infected cell. Instead, free virus is cleared at a rate of c per day.

We point out that separation of the infected cells into two populations increases the realism of the model, because delays in the production of virus after the time of initial infection are part of the viral life cycle. Furthermore, to be more focused on the process of cells decrease by the virus infection, the model (1) neglects target cells proliferation and natural death, since the infection typically exhibits a shorter timescale.

For the model (1), it is possible to compute the *basic reproduction number* R_0 as the average number of second-generation infections produced by a single infected cell initially placed in a population of entirely susceptible cells [1, 2, 4], namely

$$R_0 = \frac{p\,\beta\,T_0}{c\,\delta}\,, \qquad (2)$$

where T_0 is the number of target cells available at the starting time of the infection. If $R_0 > 1$, then an infection can actually be established and it expands exponentially according to this value, whereas it rapidly disappears if $R_0 < 1$.

We propose different simulations performed by exploiting the parameters in [1] (see Table 1). The initial number of target cells is assumed to be $T_0 = 4 \times 10^8$, which is an estimate of the number of units in the upper respiratory tract, while the experimental data for I_1 and I_2 are initially fixed to zero. The geometric average of R_0 values for the six patients in Table 1 is 21.8, suggesting that an initial infection spreads rapidly and would be difficult to extinguish.

Figure 2 shows that, near the viral titer peak, a majority of target cells has been eliminated in most of the cases. While this would seem to exclude the possibility of the infection lasting as late as 6/8 days, these simulations also suggest that, despite the few remaining target cells past the viral peak, the model can indeed sustain

infection during the predicted days (refer to the graph related to the fifth patient, for example).

Now, we briefly consider the model (1) with the usage of an antiviral drug therapy (more details are provided in Section 2). The rather large values of R_0 in Table 1 indicate that antiviral treatments need to be supplied before or very early after the infection outbreak. Thus, we focus on the clinical application with neuraminidase inhibitors (NIs) such as Zanamivir as done in [1], which are administrated at three different viral stages, in order to report the effects of both prophylactic and antiviral treatment. Since NIs prevent new virions from budding off an infected cell, their use is incorporated into the model (1) by reducing the viral production rate (p), and thus the corresponding basic reproduction number (2). Comparing the results of these new simulations with experimental data in [8], reasonable agreement is obtained when a reduction of viral production p of 97% is set [1].

Figure 3 shows the simulation outcomes according to this change in the values of p. The other parameters describing the infection without therapy are V_0 = 0.25 TCID50/ml, $\beta = 1.4\times10^{-2}d^{-1}(TCID50/ml)^{-1}$, $k = 3.2d^{-1}$, $\delta = 3.2d^{-1}$, $p = 2.7x10^{-5}$ $d^{-1}TCId50/ml$, $c = 3.2$ d^{-1}, and these values are hold constant except for p, which is then set to $0.03 \times p$ from the time of drug administration onwards. We compare four different trends in order to express changes in the viral titer: one describes the course of infection in the absence of NIs therapy, whilst the others include the usage of NIs at different stages, more precisely 0, 1.2 and 2.08 (days) after the beginning of infection (referring to the preventive-treatment group, the early-treatment group and the delayed-treatment group, respectively). In all cases, the virus is predicted to be cleared before an infection can become established, consistently with clinical results in [8]. Thus, treatment of Influenza A virus infection with NIs should reduce the period of symptomatic disease and, furthermore, prophylactic usage with a highly effective NI is predicted to prevent infection.

Another model considered in [1] takes account of the infected cells as a unique population, instead of dividing them into two different subpopulations I_1 and I_2, thus also reducing the number of experimental parameters. This representation does not contemplate the delay in viral production (eclipse phase), which actually makes the model (1) more realistic. We point out that the effects of immune response are not explicitly described in the simple model (1), but they are implicitly included through the death rate of infected cells (δ) and the clearance rate of virus (c). Thus, the infection resolution is a direct consequence of the target cells limitation. However, clinical reports from immunocompromised humans who shed Influenza A virus for prolonged periods suggest that the immune response plays a crucial role in clearing the infection, or at least in preventing it from becoming chronic and potentially lethal. Hence, we also make reference to relevant modifications of the model (1) which include the innate immune response component [1], or both the innate and adaptive ones [6, 7, 15].

Another variation of the model (1) is proposed in [1] by implementing the following delay differential equation:

$$\frac{dF}{dt} = sI_2(t-\tau) - \alpha F\,, \qquad (3)$$

in order to incorporate the important role played for the Influenza A virus infection by the interferons (IFN), a group of signaling proteins released by the host cells in response to the presence of various viruses. Therefore, it is assumed that IFNs are secreted from virus-producing cells (I_2) at a rate s (per cell), but starting τ time units after cells begin producing virus; moreover, this amount is proportional to that made collectively by infected cells, monocytes, macrophages and plasmacytoid dendritic cells. The constant parameter α represents the loss rate of IFNs, either by binding to cellular IFN receptors or through degradation.

This modification allows to explain the emergence in some patients of two virus titer peaks, which were absent in the simulations of the original model (see Figure 2). The bimodal virus titer curves are a phenomenon already observed in several studies [11, 12, 13], either using the average virus titer of patients involved or taking the individual value for each patient (in this last case, the bimodal virus titer was present in about half of the patients). In fact, the bimodal virus titer curves in Figure 4 have been obtained by numerically simulating the model in [15], which includes the innate response as the interaction between IFNs and the target cells, and the immune response through the action of *Natural Killer cells*, always activated by the IFNs. Indeed, because of the presence of IFNs, the uninfected

target cell count decreases, since the cells become refractory to infection, whereas the Natural Killer cells induce cytolysis of infected epithelial cells. In this case, the bimodal characteristic of the virus titer curves could be due to the IFNs dynamics, which peaks shortly after the first viral peak, and then decreases rapidly, so that the second viral titer peak can be explained by the loss of the IFN-induced antiviral effect.

Nevertheless, the model (1) together with equation (3) is affected by some limitations, especially for the larger number of parameters compared to the lower amount of experimental data available for human influenza infections. On the contrary, studies on animals usually provide more data. The availability of additional data for immunocompromised animals, as well as data for dead cells and immune response components, has allowed to make further progress in discriminating between different possible models for the infection dynamics [7, 15]. These studies conclude that both an innate and an adaptive immune response component is required to properly describe the infection dynamics and, therefore, to provide an adequate explanation of the observed data.

2. Numerical simulation of the effects of antiviral treatments

In that context, we consider the presence of antivirals, such as chloroquine or hydroxychloroquine.

Let ε be the effectiveness of administrated drug and, according to [4] (see also the supplementary information), assume that antivirals with an effectiveness ε work in reducing the basic reproduction number R_0 computed in (2) by a factor (1 - ε). This hypothesis can be included into the model (1) by modifying either β or p to obtain the following ordinary differential equations:

$$\begin{cases} \dfrac{dT}{dt} = -(1-\varepsilon)\beta TV \\ \dfrac{dI_1}{dt} = (1-\varepsilon)\beta TV - kI_1 \\ \dfrac{dI_2}{dt} = kI_1 - \delta I_2 \\ \dfrac{dV}{dt} = pI_2 - cV \end{cases} \tag{4}$$

and

$$\begin{cases} \dfrac{dT}{dt} = -\beta TV \\ \dfrac{dI_1}{dt} = \beta TV - kI_1 \\ \dfrac{dI_2}{dt} = kI_1 - \delta I_2 \\ \dfrac{dV}{dt} = (1-\varepsilon)pI_2 - cV \end{cases} \tag{5}$$

In order to promote an effective choice between the models (4) and (5), we have numerically simulated both systems to compare their solutions to that of the original model (1). As a matter of fact, the presence of the reducing factor (1 - ε) has a more significant impact on the dynamics of system (5), as shown in Figure 7, since a decrease of the viral load peak can be clearly observed with respect to Figure 5 and Figure 6. On the contrary, reducing the infection rate β by the factor (1 - ε) does not produce any relevant effect on the overall dynamics, and there is a complete coincidence of the numerical simulations of the models (1) and (4), as shown in Figure 5 and Figure 6, respectively. This particular behavior might be explained by the fact that the parameter β appears inside the equations always multiplied by the variable T, which from an initial value T_0 of the order of 10^8 (refer to Section 2) drops rapidly toward zero (in an extremely short time), thus making the effect of the infection rate β negligible as soon as T vanishes From a mathematical point of view, the initial datum T_0 plays the role of a *stiffness parameter* for the model (1) and its variants (4) and (5), leading to the appearance of *fast-slow dynamics* usual ly reported for multiscale nonlinear processes [18].

Then, we focus our attention on the effectiveness ε of antivirals, by studying how this factor eventually changes with time. Following the hypothesis made by Gonçalves et al. [4], we assume that the effectiveness of a treatment, at some time t after its administration has begun, is related to the plasma total drug concentration C through the empirical law given by

$$\varepsilon(t) = \frac{C(t)}{C(t) + EC_{50}}, \tag{6}$$

where EC_{50} is the drug concentration typically required to produce 50% of its maximal effect during a given time interval. This is an intrinsic PharmacoKinetics (PK) drug property, representing the drug's generic po

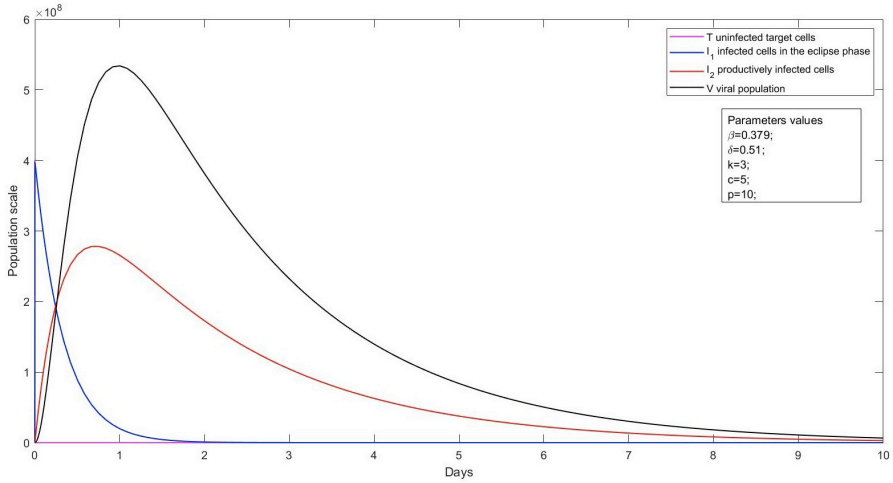

Figure 5: Target cell-limited model (1) without antiviral effects.

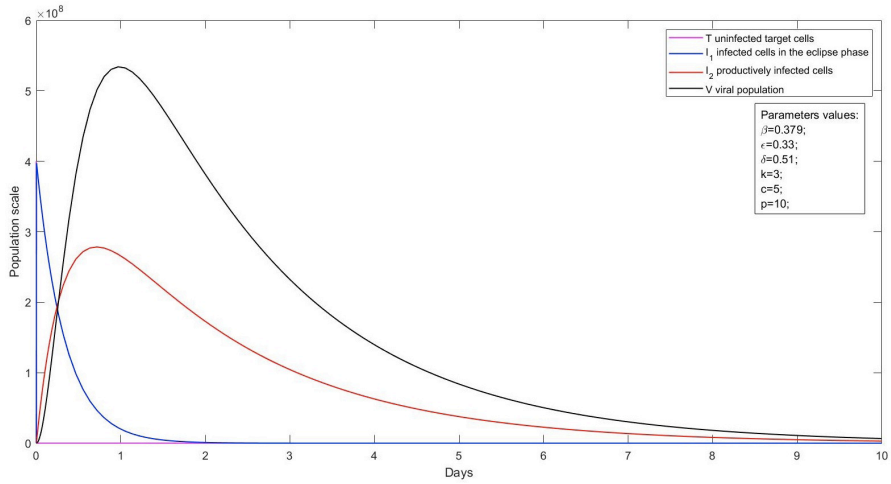

Figure 6: Target cell-limited model (4) with the reducing factor (1-ε) to simulate antiviral effects on the infection rate β.

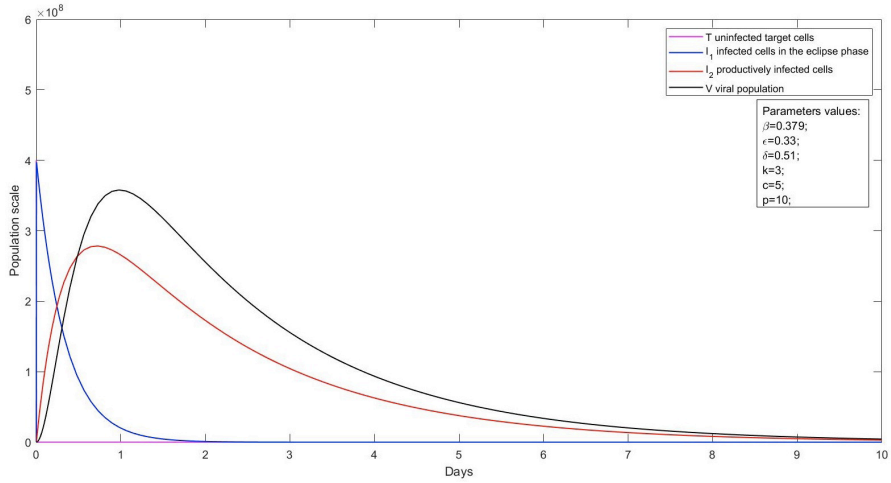

Figure 7: Target cell-limited model (5) with the reducing factor(1-ε) to simulate antiviral effects on the viral production p.

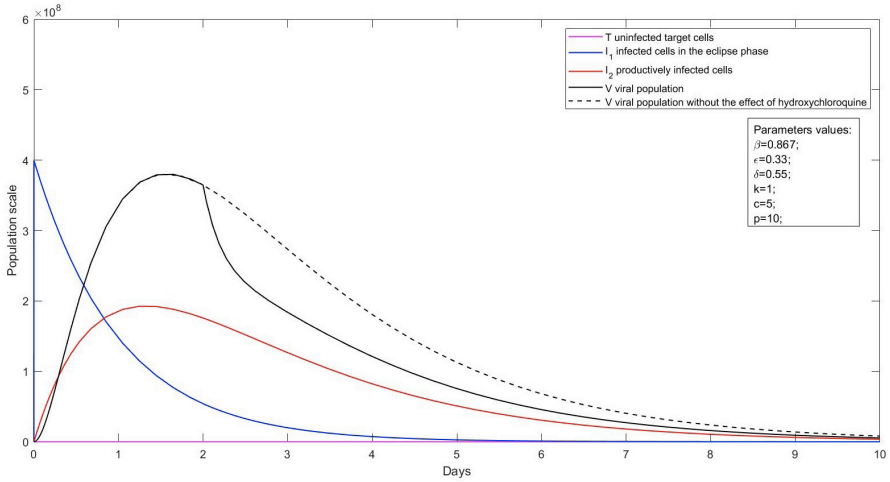

Figure 8: Simulation with hydroxychloroquine administrated 2 days after the infection outbreak.

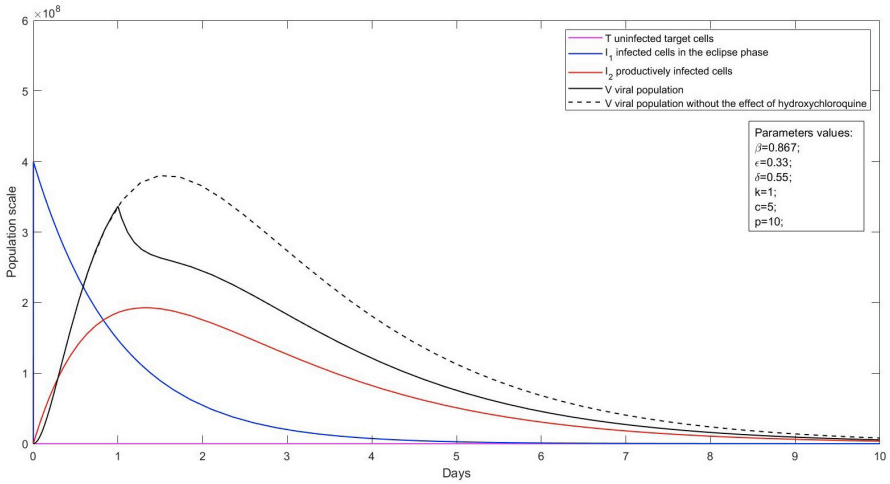

Figure 9: Simulation with hydroxychloroquine administrated 1 day after the infection outbreak.

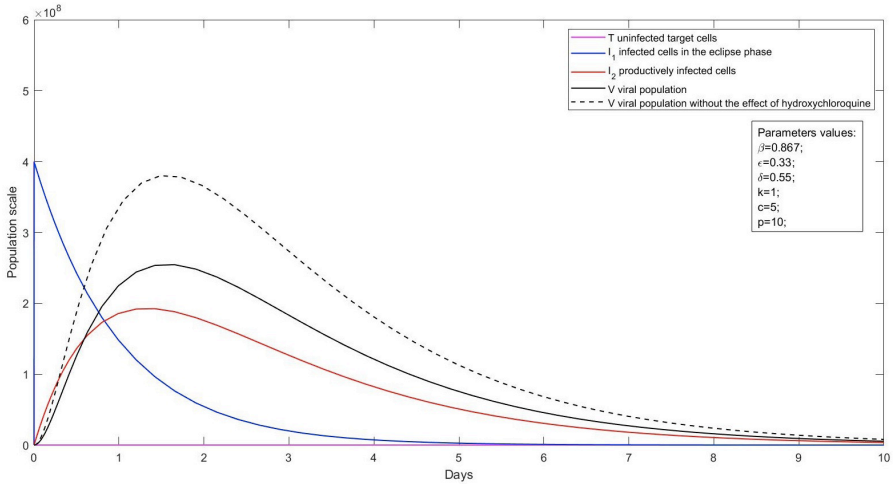

Figure 10: Simulation with hydroxychloroquine administrated at the infection outbreak.

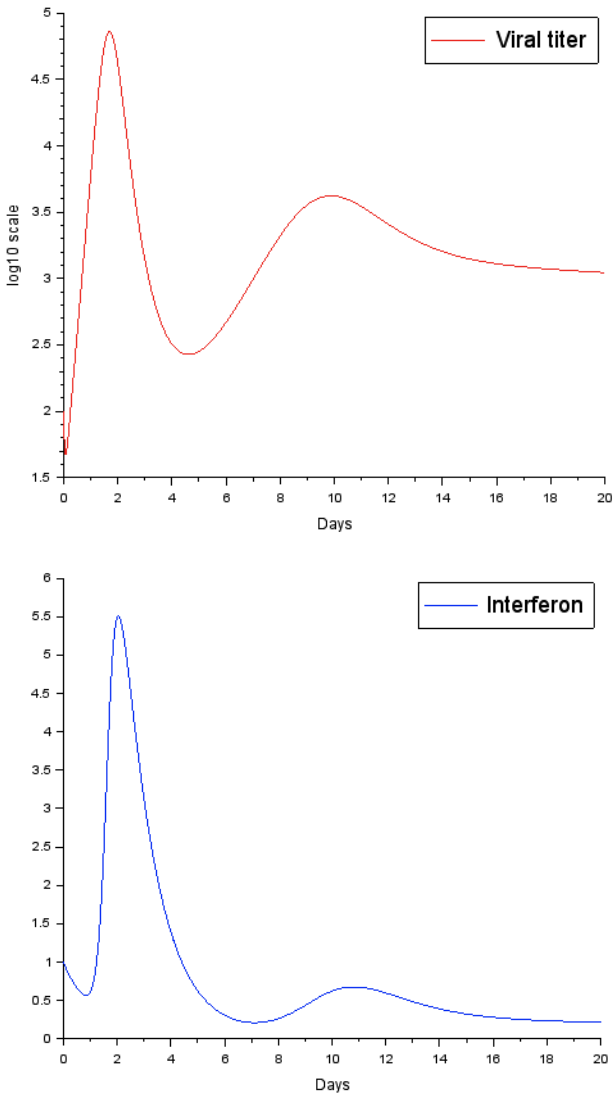

Figure 4: Simulation of viral titer double peaks obtained by using the target cell-limited model with IFNs action proposed in [15] (this model with differential delay does not consider the eclipse phase of infected cells). The graphs illustrate the viral titer curve (red) with two peaks and the INF dynamics (blue) during the course of the infection.

tency: among drugs which have effect on the same receptor system, the ones with lower values of EC_{50} are more powerful.

More specifically for chloroquine and hydroxychloroquine, experimental results from *in vitro* studies have proven that both have good antiviral activity [17, 20, 5]. In particular, it has been found in [21] that they are able to decrease the viral replication depending on their concentration, and therefore we can assert that the expression in (6) correctly describes this phenomenon, because the decrease of viral replication is ε-dependent and ε is itself concentration-dependent. Once a mathematical model of viral dynamics has been fitted to experimental data, we can combine the estimates of viral replication parameters with the specific properties of the drug candidates, in order to formulate possible conclusions regarding the effects of the treatments for various dosing regimens [4]. For that issue, we consider the EC_{50} value of the drugs under investigations during various time intervals. According to [21], the EC_{50} values for chloroquine are 23.90 μM and 5:47 μM at 24 hours and 48 hours after the administration, respectively; on the other hand, the EC_{50} values for hydroxychloroquine are 6.14 μM and 0.72 μM at 24 hours and 48 hours after the administration, respectively. Hence, we conclude that hydroxychloroquine exhibits a superior *in vitro* antiviral effect in comparison to chloroquine and, from now on, we consider only results concerning the treatment based on hydroxychloroquine. For the experimental setting, following the approach by Gonçalves et al. [4], we take into account published data from four different Singapore hospitals, to run and examine several simulations concerning hydroxychloroquine efficiency. The patients from the trial group (13 patients) were hospitalized, on average, 3 days after the onset of symptoms (range of the real data: 1-10 days) and had not yet started any treatment. Adopting the real time Reverse Transcription Polymerase Chain Reaction (RT PCR) technique, viral loads in nasopharyngeal swabs, to which patients have been tested, were measured at multiple time points. The observed data showed a peak of viral load at 5 days after the onset of symptoms, on average (range of the real data: 2-27 days).

As the parameter values of our simulations, we assume the initial target cell concentration to be 1.33 x 10^7 cells/ml distributed over 30 ml of nasopharyngeal volume, which gives a total number T_0 = 4 x 10^8 of nasopharyngeal target cells. Following previous models of viral infection [2], we consider the clearance rate of virus as c = 5 d^{-1} and virions are supposed to be released from infected cells (I_2) at rate p = 10 d^{-1}. When data availability is limited to the viral loads, not all parameters can be estimated. For this reason, several values of k were tested in [4], recalling that all the data from Computed Tomography (CT) were reported into a $\log_{10}$ scale, since this transformation does not change the quality of the parameters to be identied. The values $\{k_1, k_2, k_3\}$ = {1, 3, 5} d^{-1} provide good fitting of the model, therefore we use the estimates deduced from them for the remaining parameters (refer to [4] for supplemental information). In particular, we choose the death rate of productively

infected cells as $\{\delta 1, \delta 2, \delta 3\} = \{0.55, 0.51, 0.52\}$ d^{-1} (consequently, the average life span is about 1.88, 1.96 and 1.92 days, respectively) and the (normalized) infection rate as $\{\beta 1, \beta 2, \beta 3\} = \{0.867, 0.379, 0.302\}$. For each set of different parameters, we calculate the basic reproduction number R_0 which is found to take the values 27.1, 12.8 and 10.0, respectively. The mean antiviral effectiveness of a drug in seven days of treatment is given by the integral formula, namely

$$\overline{\varepsilon} = \frac{1}{7}\int_0^7 \frac{C(t)}{C(t)+EC_{50}}dt\,. \qquad (7)$$

Concerning the COVID-19, the characteristic value of $\overline{\varepsilon}$ is about 33% for the hydroxychloroquine [4], and we used this value as parameter ε in our numerical simulations. We analyze how the hydroxychloroquine treatment affects the viral load peak when the drug is administrated at different times after the infection outbreak, with the set of parameters related to $k = 1$.

All the figures show an early viral load peak followed by a progressive decrease of the virions. According to the experimental data, the value of this peak without any treatment is about 3.8 x 10^8 and it occurs about 36 hours after the infection outbreak (dashed line).

The action of hydroxychloroquine reduces the viral load in different ways, depending on when the treatment is administrated: for instance, providing the hydroxychloroquine 2 days after the infection outbreak helps the abatement of the viral load, but it does not have any effect on the peak intensity (see Figure 8). Instead, initializing the treatment 1 day after the infection outbreak reduces the viral load peak to about 3.4 x 10^8 (see Figure 9). Finally, we observe the most signicant effect when the hydroxychloroquine is administrated immediately at the infection outbreak, and in this case the peak value decreases to about 2.5 x 10^8 (see Figure 10).

We deduce from these results that hydroxychloroquine does not have relevant antiviral effects if administrated more than 2 days after the infection outbreak. Indeed, it is advisable to initialize the treatment earlier, sometimes as a prophylactic agent to decrease the viral load peak, thus attenuating the viral replication and mitigating the disease progression, even if it could be not a complete protection.

However, it is worthwhile noticing that the correction by the factor $(1-\varepsilon)$ of parameter p modifies only the behavior of the variable V, while leaving completely unchanged the others. This is justied by observing that parameter p is present only in the last equation of the model (1) and its variants, and then V appears in the first two equations, but always multiplied by the variable T which, as already explained, rapidly goes to zero (in almost an infinitesimal time). Following a purely qualitative approach, we simplify the model (5) by considering $T(0) = 0$ (hence $T(t) = 0$ is a stable solution to the first equation), and we solve the remaining (triangular) system, for $I_1(0) \neq 0$ in order to initialize the dynamics, together with $I_2(0) = 0$ and $V(0) \neq 0$, so that we obtain the following explicit solution:

$$\begin{cases} I_1(t) = I_1(0)\,e^{-kt} \\ I_2(t) = I_1(0)\dfrac{k}{k-\delta}\left(e^{-\delta t} - e^{-kt}\right) \\ V(t) = V(0)\,e^{-ct} \\ \qquad + I_1(0)\dfrac{k}{c-\delta}\cdot\dfrac{(1-\varepsilon)p}{k-\delta}\left(e^{-\delta t} - e^{-ct}\right) \\ \qquad - I_1(0)\dfrac{k}{c-k}\cdot\dfrac{(1-\varepsilon)p}{k-\delta}\left(e^{-ct} + e^{-kt}\right) \end{cases} \qquad (8)$$

Therefore, the parameter p and its reducing factor $(1 - \varepsilon)$ determine only the dynamics of the variable V from (8), and the difference between the numerical simulations with or without the hydroxychloroquine effects is observable only in the behavior of V.

In conclusion, we have to point out that our model is not really predictive: indeed, the simulations above show the viral peak already after 1 - 2 days, differently from the average period of 5 days actually observed for the 13 patients analyzed in [4]. In order to become more realistic, an agreement is necessary on both the parameters to be used and their appropriate estimate to be inserted into the numerical algorithm, because the models presented in this article are highly unstable with respect to the initial data. Rigorous studies on these aspects are still under development, as well as those related to hydroxychloroquine and its experimentation as a medicinal product for the SARS-CoV-2 virus. In fact, all these qualitative results are valid under the hypothesis that the treatments act according to the modeling assumptions, we seems not to unanimously confirmed by recent studies [3, 21].

Acknowledgments

The authors thank the Department of Mathematics G. Castelnuovo, Sapienza University of Rome, for having hosted the electronic workshop "COVID-19 calls for Mathematics" www1.mat.uniroma1.it/ricerca/ convegni/2020/COVIDchiamaMAT – which has motivated this project. This project is partially supported by the French government, managed by the ANR under the UCA JEDI Investments for the Future project, reference no. ANR-15-IDEX-01.

References

1. Baccam, P, Beauchemin, C, Macken, CA, Hayden, FG & Perelson, AS 2006, "Kinetics of influenza A virus infection in humans", *Journal of Virology*, vol. 80, no. 15, pp. 7590-7599.
2. Best, K, Guedj, J, Madelain, V, de Lamballerie, X, Lim, SY, Osuna CE, Whitney JB & Perelson AS 2017, "Zika plasma viral dynamics in nonhuman primates provides insights into early infection and antiviral strategies", *Proceedings of the National Academy of Sciences*, vol. 114, no. 33, pp. 8847-8852.
3. Geleris, J, Sun, Y, Platt, J, Zucker, J, Baldwin, M, Hripcsak, G, Labella, A, Manson, D, Kubin, C, Barr, RG, Sobieszczyk, ME & Schluger, NW "Observational study of hydroxychloroquine in hospitalized patients with Covid-19", *The New England Journal of Medicine*, preprint www.nejm.org/doi/full/10.1056/NEJMoa201241010.1056/NEJMoa2012410
4. Gonçalves, A, Bertrand, J, Ke, R, Comets, E, de Lamballerie, X, Malvy, D, Pizzorno, A, Terrier, O, Calatrava, MR, Mentrè, F, Smith, P, Perelson, AS & Guedj, J, 2020, "Timing of antiviral treatment initiation is critical to reduce SARS-Cov-2 viral load", medRxiv preprint http://doi.org/10.1101/2020.04.04.20047886v1
5. Haladyj, E, Sikora, M, Felis-Giemza, A & Olesinska, M, 2018, "Antimalarials: are they effective and safe in rheumatic diseases?", *Reumatologia*, 56 (3): 164-173.
6. Handel, A, Longini, I Jr & Antia, R 2007, "Neuraminidase inhibitor resistance in influenza: assessing the danger of its generation and spread", *PLoS Computational Biology*, vol. 3, no. 12, pp. 2456-2464.
7. Handel, A, Longini, I Jr & Antia, R 2010, "Towards a quantitative understanding of the within-host dynamics of influenza A infections", *Journal of the Royal Society Interface*, vol. 7, no. 42, pp. 35-47.
8. Hayden, FG, Treanor, JJ, Betts, RF, Lobo, M, Esinhart, J.D. & Hussey E.K. 1996, "Safety and efficacy of the neuraminidase inhibitor GG167 in experimental human influenza", *Journal of American Medical Association*, vol. 275, no. 4, pp. 295-299.
9. Hu, TY, Frieman, M & Wolfram, J 2020, "Insights from nanomedicine into chloroquine efficacy against COVID-19", *Nature Nanotechnology*, vol. 15, pp. 247-249.
10. Inoue, Y, Tanaka, N, Tanaka, Y, Inoue, S, Morita, K, Zhuang, M, Hattori, T & Sugamura, K 2007, "Clathrin-dependent entry of Severe Acute Respiratory Syndrome Coronavirus into target cells expressing ACE2 with the cytoplasmic tail deleted", *Journal of Virology*, vol. 81, no. 16, pp. 8722-8729.
11. Jao, RL, Wheelock, EF & Jackson, GG 1970, "Production of interferon in volunteers infected with Asian influenza", *Journal of Infectious Diseases*, vol. 121, no. 4, pp. 419-426.
12. Murphy, BR, Chanock, RM, Douglas, RG, Betts, RF, Waterman, DH, Holley Jr, HP, Hoover, DL, Suwangool, S, Nalin, DR & Levine, MM1980, "Temperature-sensitive mutants of influenza A virus: evaluation of thevAlaska/77-ts- 1A2 temperature-sensitive recombinant virus in seronegative adult volunteers", *Archives of Virology*, vol. 65, no. 2, pp. 169-173.
13. Murphy, BR, Rennels, MB, Douglas Jr, RG, Betts, RF, Couch, RB, Cate, TR,WC, Chanock, RM, Kendal, AP, Maassab, HF, Suwanagool, S, Sotman, SB, Cisneros, LA, Anthony, Nalin, DR & Levine, MM 1980, "Evaluation of influenza A/Hong Kong/123/77 (H1N1) ts-1A2 and cold adapted recombinant viruses in seronegative adult volunteers", *Infection and Immunity*, vol. 29, no. 2, pp. 348-355.
14. Miller, SE, Mathiasen, S, Bright, NA, Pierre, F, Kelly, BT, Kladt, N, Schauss, A, Merrifield, CJ, Stamou, D., Honing, S & Owen, DJ 2015, "CALM regulates clathrin-coated vesicle size and maturation by directly sensing and driving membrane curvature", *Developmental Cell*, vol. 33, no. 2, pp. 163-175.
15. Pawelek, KA, Huynh, GT, Quinlivan, M, Cullinane, A, Rong, L & Perelson, AS 2012, "Modeling within-host dynamics of Influenza virus infection including immune responses", *PLoS Computational Biology*, vol. 8, no. 6, e1002588.
16. Pelt, J, Busatto, S, Ferrari, M, Thompson, EA, Mody, K & Wolfram, J 2018, "Chloroquine and nanoparticle drug delivery: a promising combina-

tion", *Pharmacology and Therapeutics*, vol. 191, pp. 43-49.

17. Savarino, A, Boelaert, JR, Cassone, A, Majori, G & Cauda, R 2003, "Effects of chloroquine on viral infections: an old drug against today's disease?", *Lancet Infect. Dis.*, vol. 3, no.11, pp. 722-727.
18. Smith, AM, Adler, FR & Perelson, AS 2010, "An accurate two-phase approximate solution to an acute viral infection model", *Journal of Mathematical Biology*, vol. 60, no. 5, 711-726.
19. Tarek, M & Savarino, A 2020, "Pharmacokinetic bases of the hydroxychloroquine response in COVID-19: implcations for therapy and prevention", medRxiv preprint https://doi.org/10.1101/2020.04.23.20076471v1
20. Vincent, MJ, Bergeron, E, Benjannet, S, Bobbie, RE, Rollin, PE, Ksiazek, TG, Seidah, NG & Nichol, ST 2005, "Chloroquine is a potential inhibitor of SARS coronavirus infection and spread", *Virology Journal*, vol. 2, no. 69.
21. Yao, X, Ye, F, Zhang, M, Cui, C, Huang, B, Niu, P, Liu, X, Zhao, L, Dong, E, Song, C, Zhan, S, Lu, R, Li, H, Tan, W & Liu, D 2020, "In vitro antiviral activity and projection of optimized dosing design of hydroxychloroquine for the treatment of Severe Acute Respiratory Syndrome Coronavirus2 (SARS-CoV-2)", *Clinical Infectious Diseases*, https://doi.org/10.1093/cid/ciaa237.
22. Wang, H, Yang, P, Liu, K, Guo, F, Zhang, Y, Zhang, G & Jiang, C 2008, "SARS coronavirus entry into host cells through a novel clathrin and caveolae-independent endocytic pathway", *Cell Research*, vol. 18, no. 2, pp. 290-301.
23. Wolfram, J, Nizzero, S, Liu, H, Li, F, Zhang, G, Li, Z, Shen, H, Blanco, E & Ferrari, M 2017, "A chloroquine-induced macrophage preconditioning strategy for improved nanodelivery", *Scientific Reports*, vol. 7, no. 1, 13738.
24. Wolfram, J & Ferrari, M 2019, "Clinical Cancer Nanomedicine", *Nano Today*, vol. 25, pp. 85-98.